Supporting information for

Synergistic Multimodal Cancer Therapy Using Glucose Oxidase@CuS Nanocomposites

Parbeen Singh,[‡a, b] Brian Youden,[‡c, d] Yikun Yang,[e] Yongli Chen,[a, b] Andrew Carrier,[c] Shufen Cui,[b] Ken Oakes,[f] Mark Servos,[d] Runqing Jiang,*[g] and Xu Zhang*[c]

[a] Postdoctoral Innovation Practice Base, Shenzhen Key Laboratory of Fermentation, Purification and Analysis, Shenzhen Polytechnic, Shenzhen, 518055, China.

[b] Department of Biological Applied Engineering, Shenzhen Key Laboratory of Fermentation, Purification and Analysis, Shenzhen Polytechnic, Shenzhen, 518055, China.

[c] Department of Chemistry, Cape Breton University, 1250 Grand Lake Road, Sydney, Nova Scotia, B1P 6L2, Canada.

[d] Department of Biology, University of Waterloo, 200 University Ave W, Waterloo, Ontario, N2L 3G1, Canada.

[e] National Cancer Center/National Clinical Research Center for Cancer/Cancer Hospital & Shenzhen Hospital, Chinese Academy of Medical Sciences and Peking Union Medical College, Shenzhen, 518116, China.

[f] Department of Biology, Cape Breton University, 1250 Grand Lake Road, Sydney, Nova Scotia, B1P 6L2, Canada.

[g] Grand River Regional Cancer Centre, 835 King St W, Kitchener, Ontario, N2G 1G3, Canada.

[‡] These authors contributed equally to this work

[*] Corresponding Authors:

Runqing.jiang@grhosp.on.ca (R. J.); Xu_zhang@cbu.ca (X. Z.).

Supporting Data

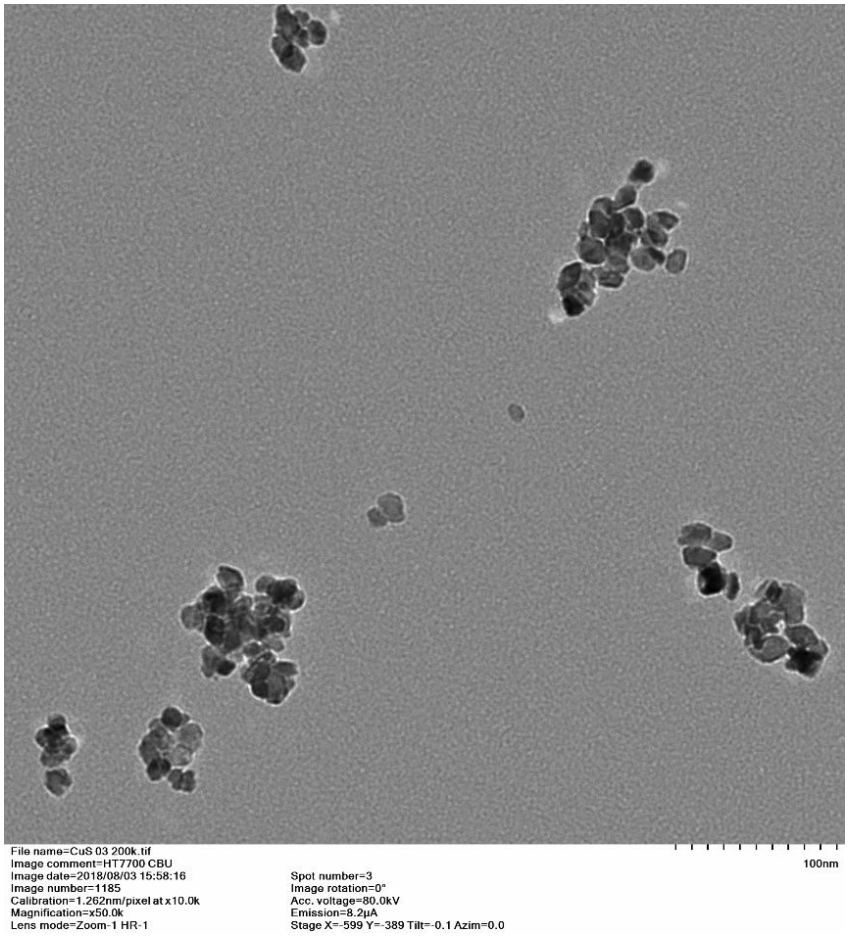

Figure S1. A transmission electron micrograph of the CuS nanoparticles.

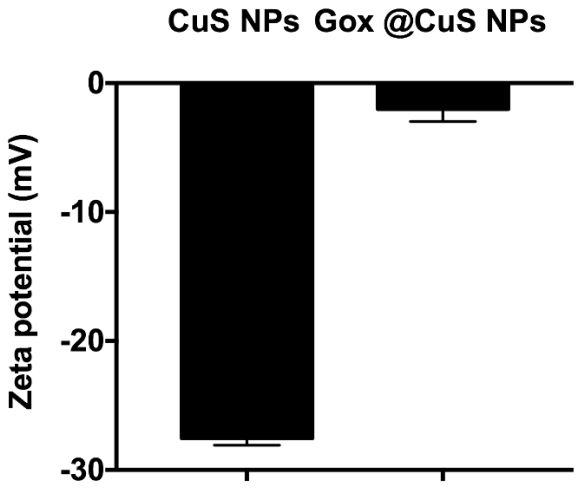

Figure S2. Zeta potentials of the CuS and Gox@CuS nanoparticles (NPs). Error bars indicate standard deviation (n = 3).

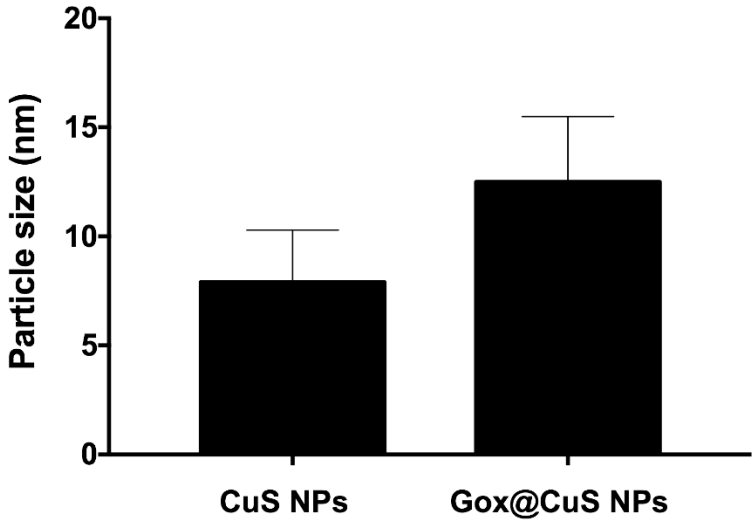

Figure S3. The hydrodynamic sizes of the CuS and Gox@CuS nanoparticles (NPs) measured by dynamic light scattering. Error bars indicate standard deviation (n = 3).

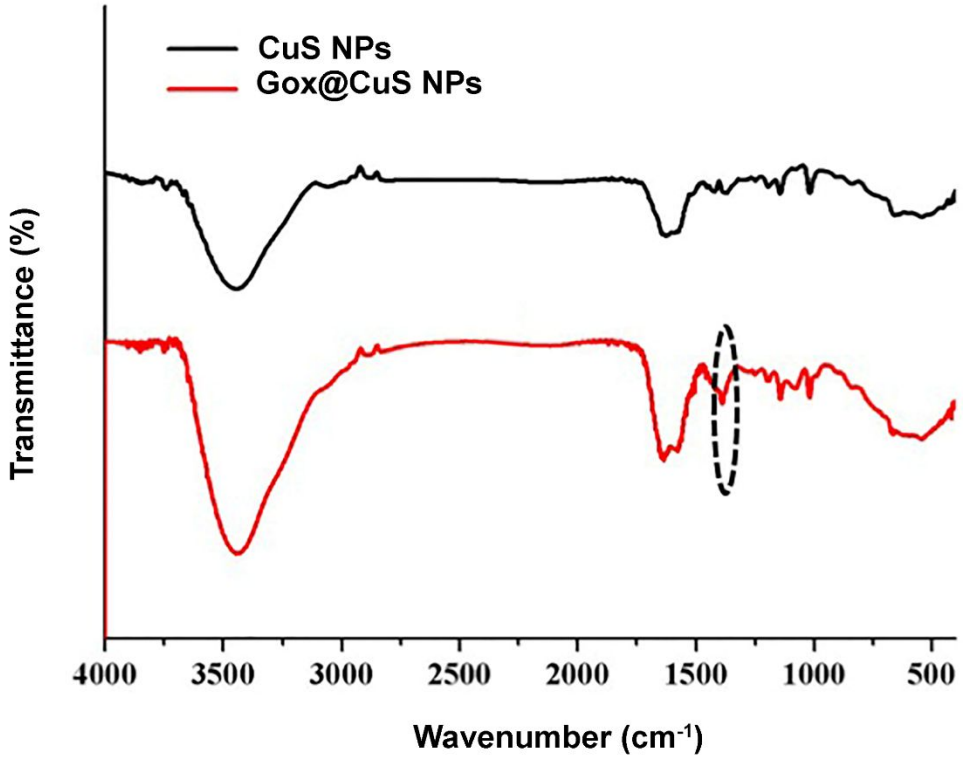

Figure S4. Fourier transform-infrared spectra of the CuS and Gox@CuS nanoparticles. The peak at 1450 cm^{-1} was assigned to C-O stretching and OH bending of Gox in the nanoparticles.

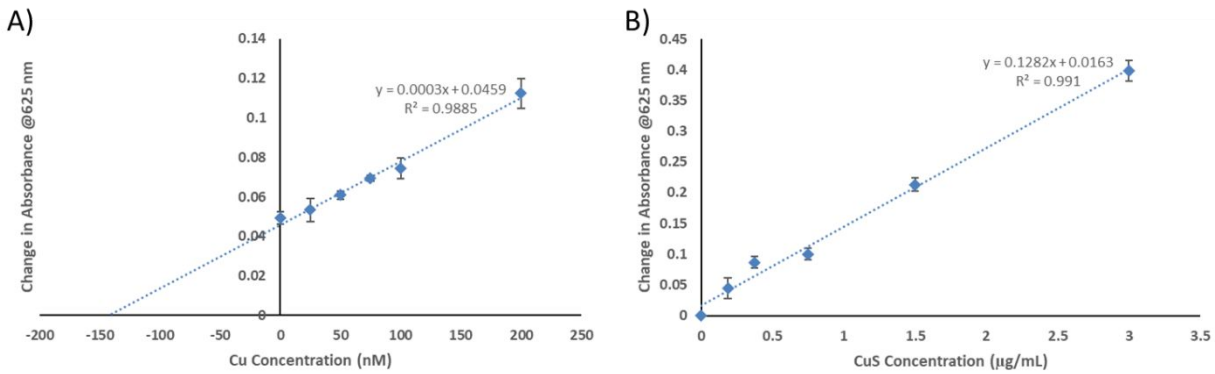

Figure S5. Quantification of copper and CuS. A) Standard addition curve for Cu^{2+} detection, and B) calibration curve for CuS detection following cellular uptake using the chloride-accelerated copper Fenton reaction with H_2O_2 and 3,3',5,5'-tetramethylbenzidine. Error bars represent standard deviation (n =3).

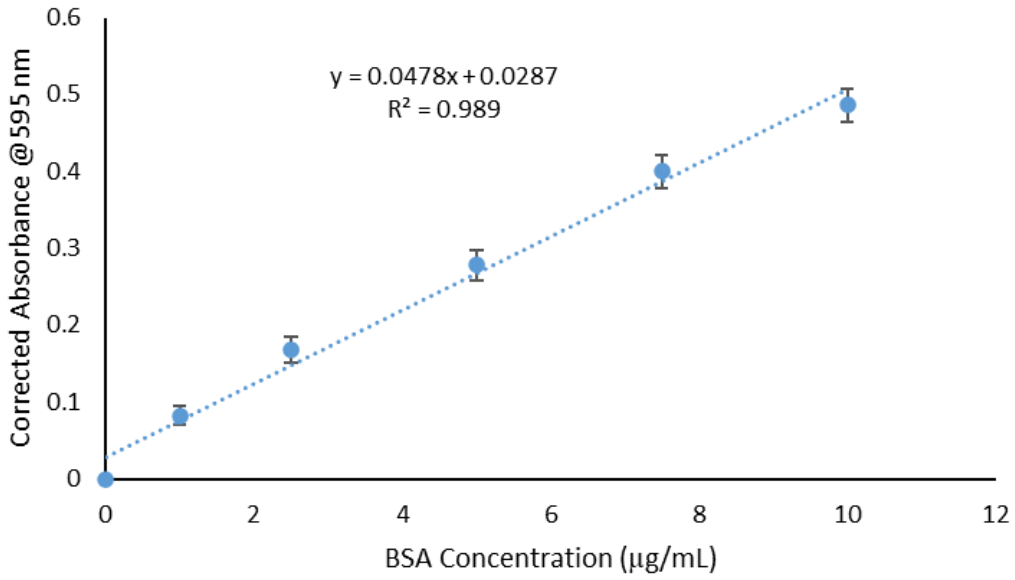

Figure S6. Standard bovine serum albumin (BSA) protein calibration curve used to quantify Gox during the Bradford assay. Error bars represent standard deviation (n =3).

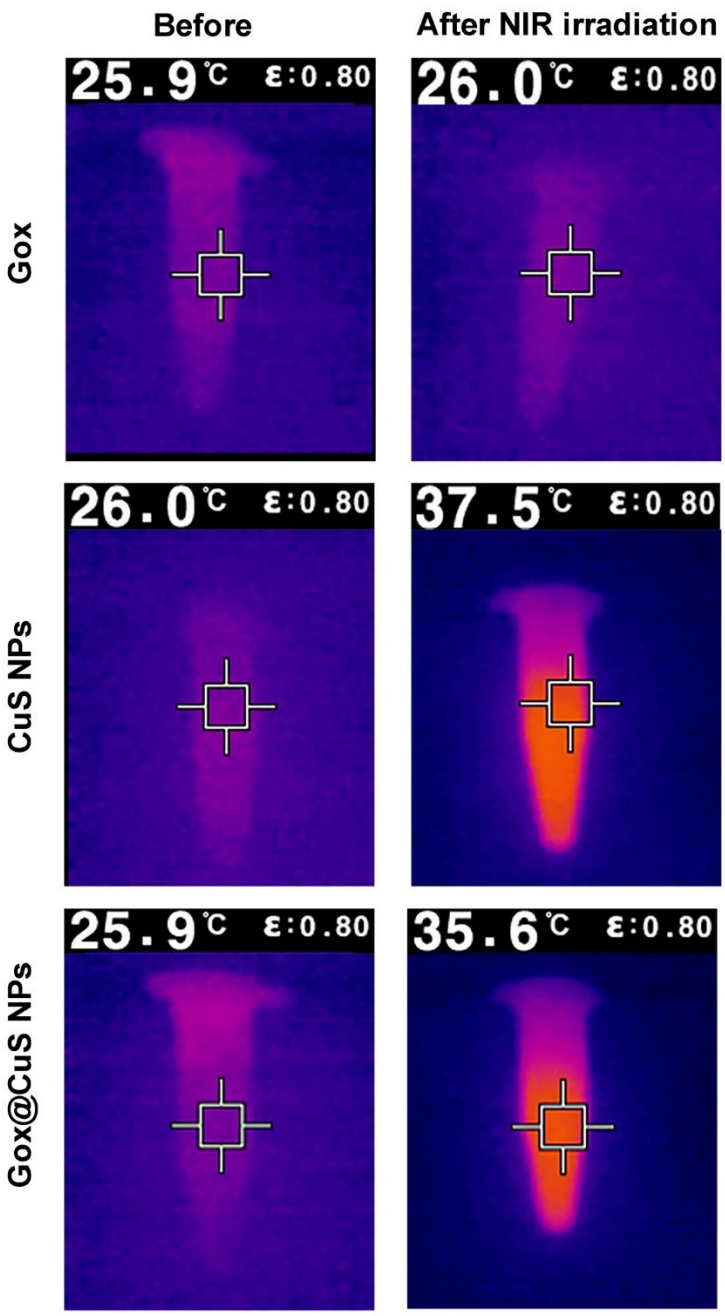

Figure S7. Infrared thermal imaging of Gox, CuS nanoparticles (NPs) and Gox@CuS NPs ([NP] = 10 μg/mL) with near infrared irradiation (980 nm, 5 W/cm^2) for 300 s.

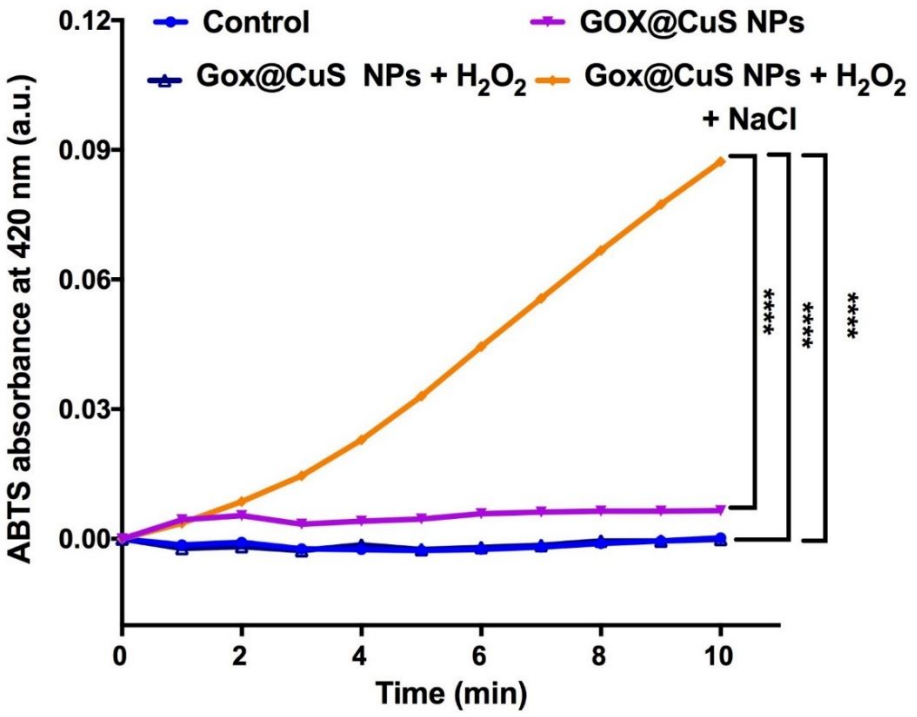

Figure S8. The Fenton catalytic activity of Gox@CuS nanoparticles (NPs). 2,2'-Azino-bis(3-ethylbenzthiazoline-6-sulfonic acid) (ABTS, 250 μM) oxidation catalyzed by Gox@CuS NPs (10 μg/mL) and H_2O_2 (200 mM) in the presence and absence of NaCl (100 mM).

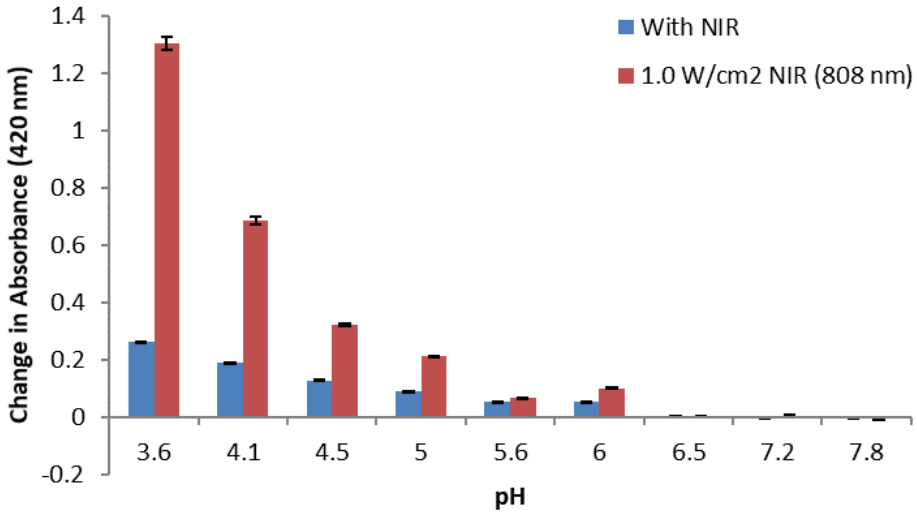

Figure S9. 2,2'-Azino-bis(3-ethylbenzthiazoline-6-sulfonic acid) (ABTS, 250 μM) oxidation catalyzed by CuS nanoparticles (10 μg/mL), NaCl (100 mM), and H_2O_2 (100 mM) at different pHs with or without near infrared (NIR) irradiation (1.5 W/cm^2). Error bars represent standard deviation (n =3).

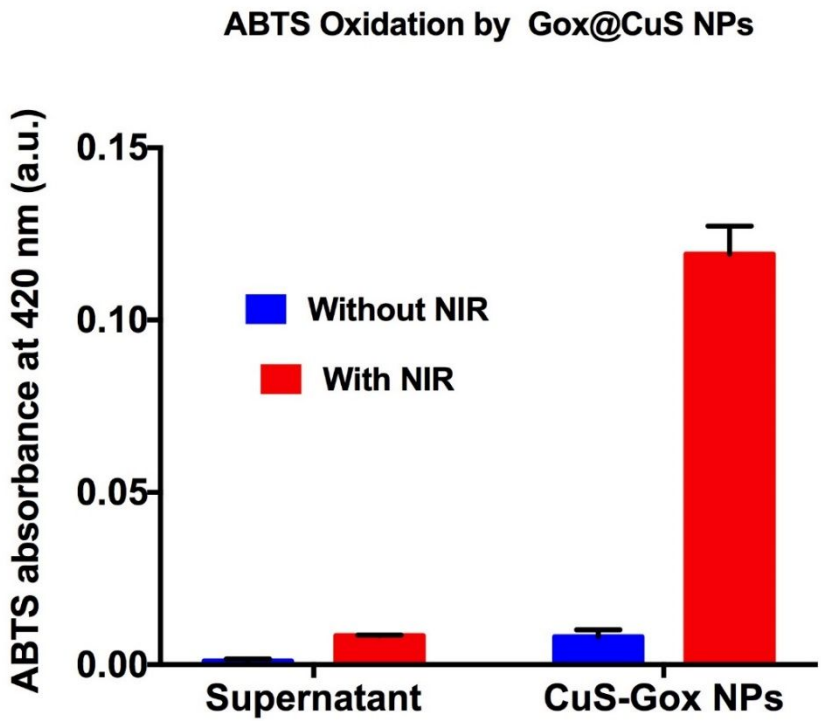

Figure S10. 2,2'-Azino-bis(3-ethylbenzthiazoline-6-sulfonic acid) (ABTS) oxidation catalyzed by Cu^{2+} leached from Gox@CuS nanoparticles (NPs) and the parent NPs with and without near infrared (NIR) irradiation. Error bars represent standard deviation (n =3).

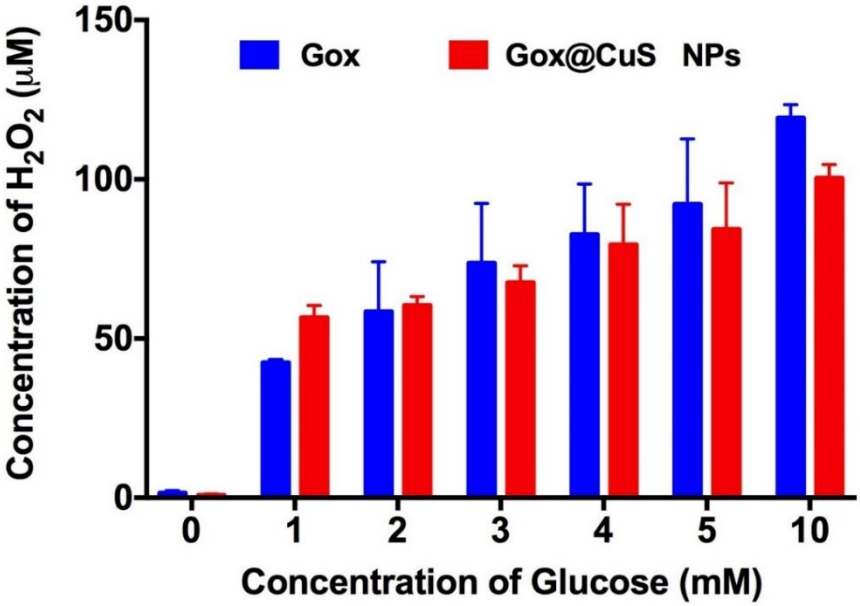

Figure S11. *In vitro* catalytic H_2O_2 production by Gox and Gox@CuS nanoparticles (NPs) with different initial glucose concentrations after 5 min. Error bars represent standard deviation (n =3).

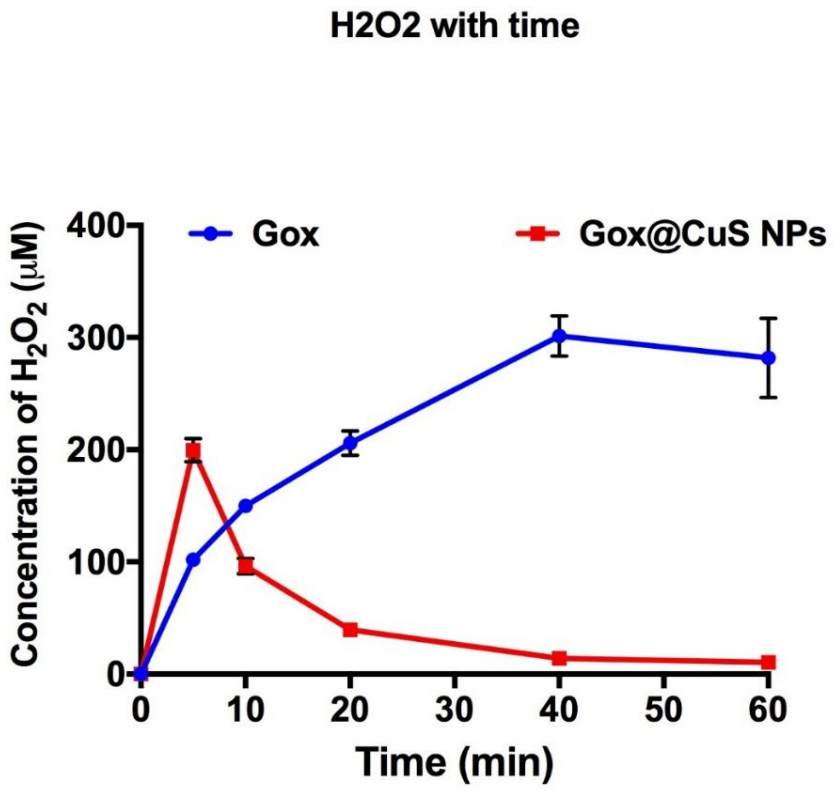

Figure S12. *In vitro* H_2O_2 generation by Gox and Gox@CuS nanoparticles (NPs) over time. CuS NPs decompose the H_2O_2 generated by glucose oxidation, producing reactive oxygen species. Error bars represent standard deviation (n =3).

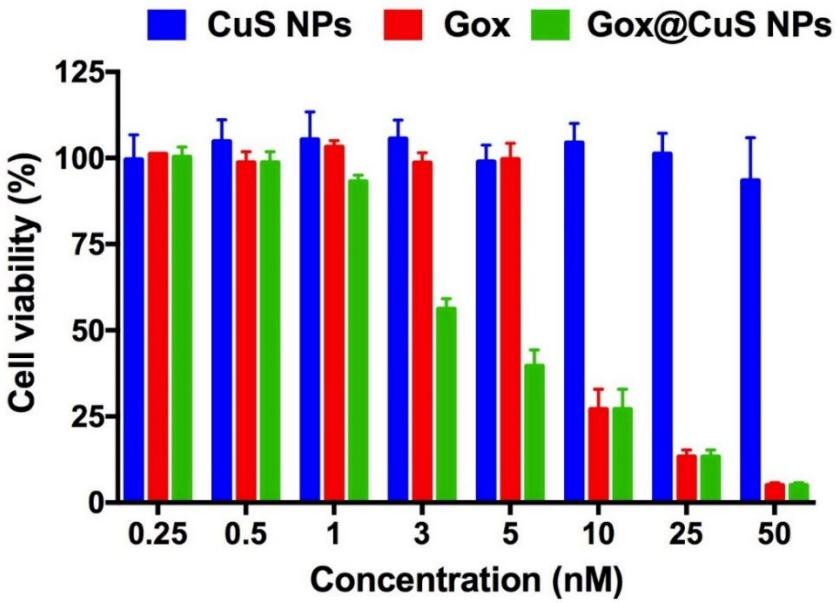

Figure S13. *In vitro* toxicity of Gox@CuS nanoparticles (NPs) in MDA-MB-231 cells. Error bars represent standard deviation (n = 3).

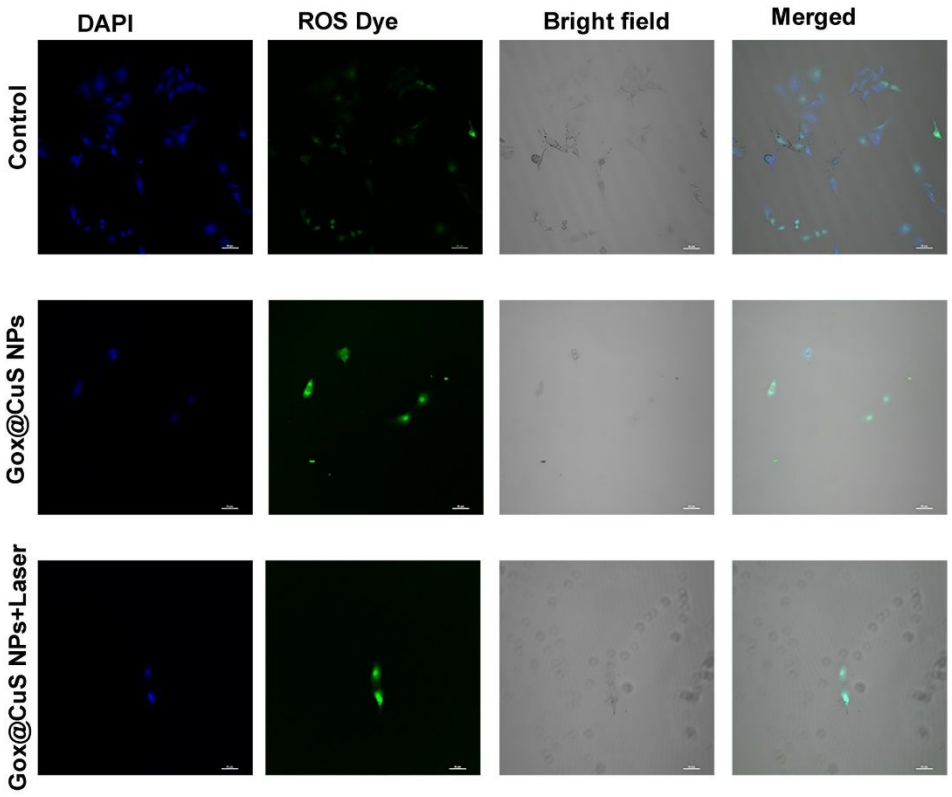

Figure S14. The intracellular reactive oxygen species (ROS) level shown by confocal laser scanning microscopy images of B16F10 cells incubated for 4 h with Gox@CuS nanoparticles (NPs) with or without a brief near infrared (NIR) irradiation (5 s). [CuS NPs] = 2 nM. Scale bars: 50 μm**.**

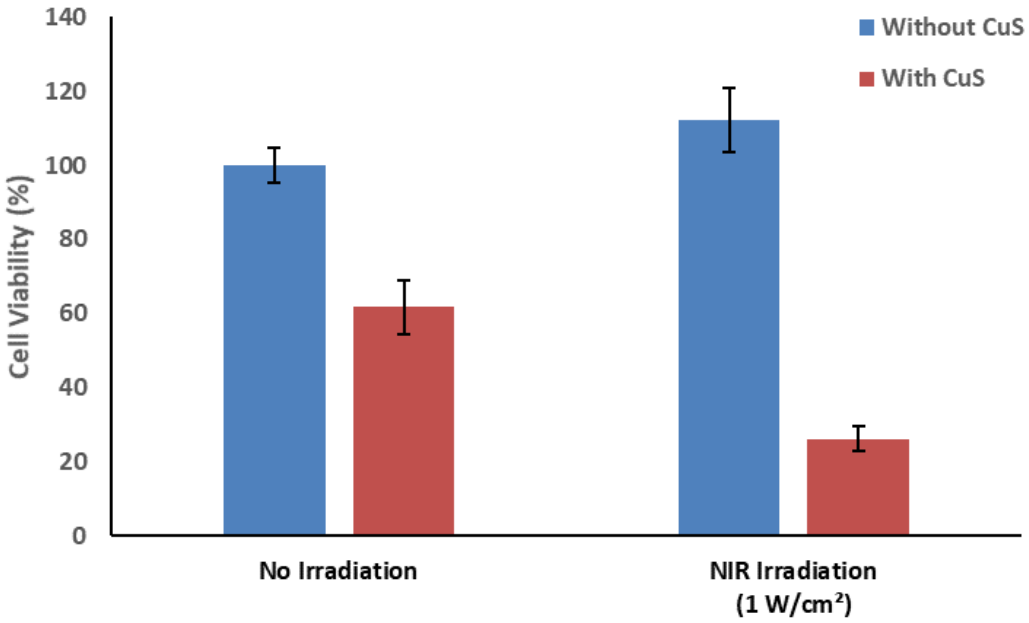

Figure S15. Cell viability of PC-3 prostate cancer cells after treatment with 30 µg/mL CuS nanoparticles (NPs) and 5 min of near infrared (NIR) irradiation (808 nm). Error bars represent standard deviation (n =3).

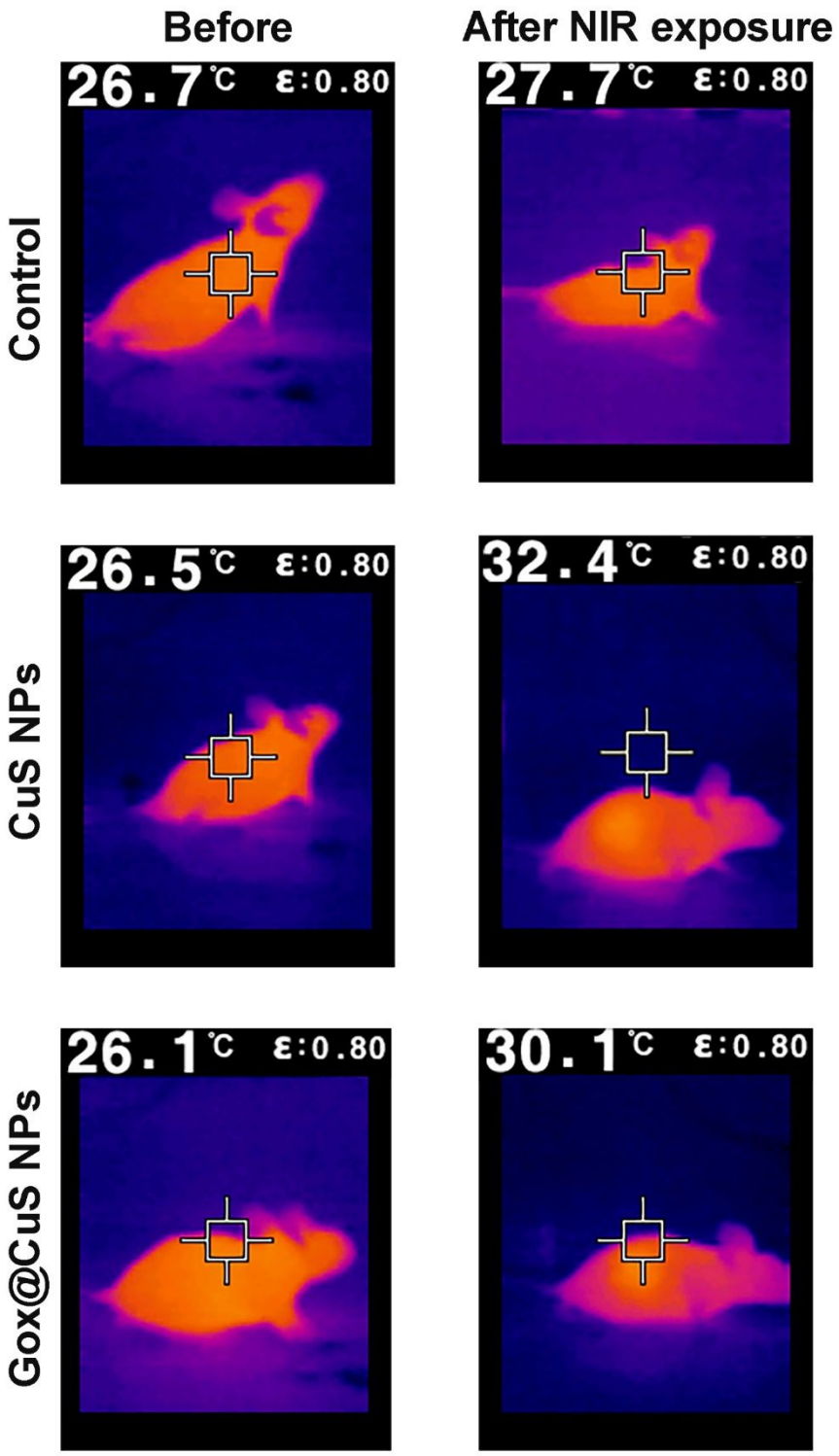

Figure S16. *In vivo* infrared thermal imaging of mice from control, CuS nanoparticle (NP), and Gox@CuS NP groups with near infrared (NIR) irradiation after drug administration ([NPs] = 200 nM, 980 nm, 5 W/cm^2 for 300 s).

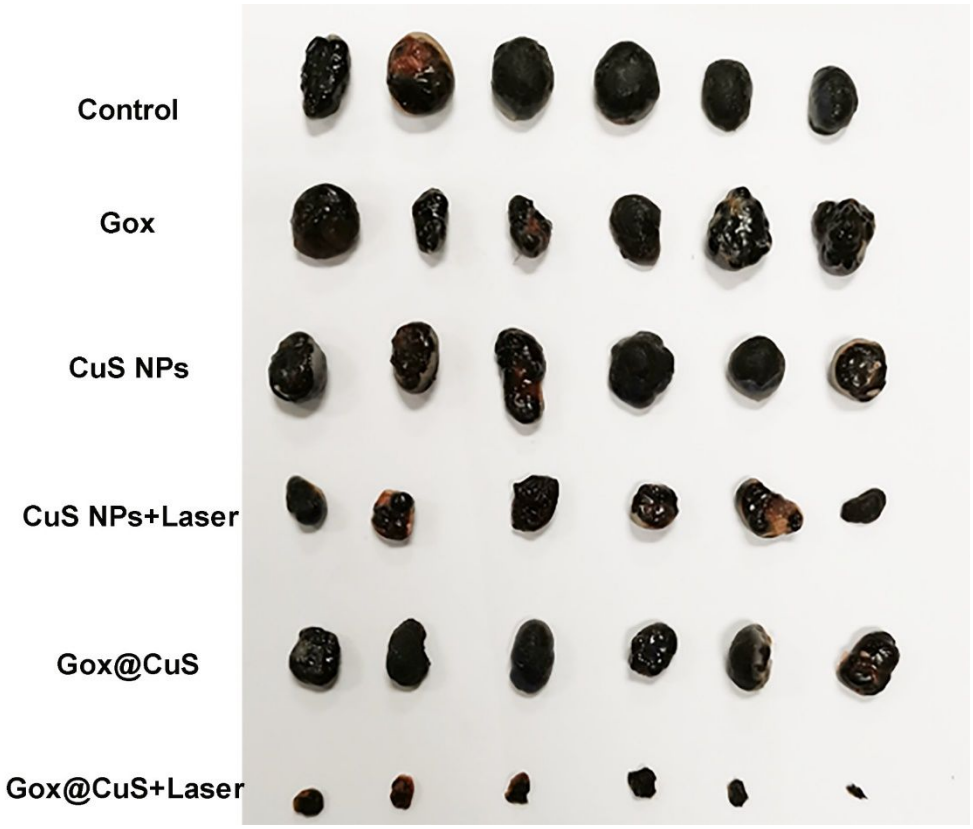

Figure S17. Therapeutic effect of Gox@CuS nanoparticles (NPs) after 10 d of treatment with almost complete eradication of the tumors.

Figure S18. Images of mice after 10 d of treatment using Gox@CuS nanoparticles (NPs) with near infrared (NIR) irradiation, showing all mice were cured with a dark black scar.

Table S1. Energy dispersive X-ray analysis of the atomic fraction of the CuS nanoparticles (NPs) and Gox@CuS NPs. (N/D: not detectable).

Metal	CuS NPs (atom%)	Gox@CuS NPs (atom%)
Cu	70	33.2
S	30	4.5
C	N/D	55.4
N	N/D	3.6
O	N/D	3.3

Table S2: Literature comparison of recent multimodal anticancer nanomedicines in terms of their methodologies and toxicities.

Reference #	Nanoformulation	Applications	In Vivo Treatment/Safety Assessments	IC50(s) (μg/mL)
Tang et al., 2020 (Theranostics)[1]	Tirapazamine and Gox encapsulated gold nanovesicles	-CDT -Starvation Therapy	-Mice euthanized after 15 d -Body weight & tumor volume -Histology	7.9–22.1 μg/mL
Deng et al., 2020 (*ACS Appl. Mater. Interfaces*)[2]	Zr-ferrocene (Fc) MOF nanosheet	-CDT -PTT	-Mice euthanized after 14 d -Body weight & tumor volume -Histology	N/A
Ma et al., 2021 (*ACS Appl. Mater. Interfaces*)[3]	Bi-Fe core-shell NP	-CDT -PDT -PTT	-Mice euthanized after 14 d -Body weight & tumor volume -Histology	N/A
Yang et al., 2020 (*ACS Nano*)[4]	Semiconducting polymer NP	-PTT -Fluorescence Imaging	-Mice euthanized after 14 & 28 d -Body weight & tumor volume -Histology	N/A
Sun et al., 2020 (*ACS Nano*)[5]	Doxorubicin (Dox)-loaded mesoporous carbon nanosphere (MnO_2 shell)	-CDT -Chemotherapy -Hypoxia relief	-Mice euthanized after 14 d -Body weight & tumor volume -Histology	N/A
Fang et al., 2020 (*Adv. Funct. Mater.*)[6]	Gox-loaded Co–fc MOFs	-CDT -Starvation Therapy	-Mice euthanized after 14 d -Body weight & tumor volume -Histology	*7–15 μg/mL
Lyu et al., 2020 (*Adv. Healthc. Mater.*)[7]	Fe_3O_4@MnO_2 core-shell nanozyme	-CDT -Hypoxia relief -MRI imaging -Radiation Therapy	-Mice euthanized after 18 d -Body weight & tumor volume -Histology	*100 μg/mL
Zhang et al., 2021	Sinoporphyrin sodium loaded-ZnO_2 NPs	-CDT -PDT	-Mice euthanized after 15 d -Body weight & tumor volume -Histology	*~0.5 μg/mL

(*ACS Appl. Mater. Interfaces*)[8]		-Fluorescence Imaging		
Ranji-Burachaloo et al., 2019 (*Nanoscale*)[9]	Gox & hemoglobin encapsulated zeolitic imidazolate framework-8 (ZIF-8) MOFs	-CDT -Starvation Therapy	N/A	1.54–17.01 μg/mL
Fan et al., 2020 (*ACS Appl. Mater. Interfaces*)[10]	Methotrexate, gadolinium, and artesunate NPs	-CDT -MRI Imaging -Chemotherapy	-Mice euthanized after 21 d -Body weight & tumor volume -Histology -Hemolysis assay -Serum analysis	9.8–19.2 μg/mL
Pu et al., 2020 (*Angew. Chem. Int. Ed.*)[11]	Iron-chelating semiconductor polymer NP	-CDT -PTT	-Mice euthanized after 14 d -Body weight & tumor volume -Histology -Hemolysis assay	N/A
Zhao et al., 2020 (*Biomaterials*)[12]	Mn-doped Gd_2O_3 NPs	-CDT -PTT -MRI Imaging	-Mice euthanized after 14 d -Body weight & tumor volume -Histology	*~25–50 μg/mL
Zhang et al., 2020 (*Chem. Eng. J.*)[13]	Dox loaded CuS@mSiO_2@MnO_2 nanocomposites	-CDT -PTT -MRI Imaging -Hypoxia Relief	-Mice euthanized after 14 d -Body weight & tumor volume -Histology	*~50–80 μg/mL
Xiao et al., 2020 (*Chem. Eng. J.*)[14]	L-Buthionine-sulfoximine modified FeS_2 NPs	-CDT -PDT -PTT -Photoacoustic Imaging -Immunotherapy	-Mice euthanized after 21 d -Body weight & tumor volume -Histology -Serum analysis	*~5–10 μg/mL Fe
Zhang et al., 2021 (*J. Colloid Interface Sci.*)[15]	Chlorin e6 (Ce6)/Gox@ZIF-8/polydopamine@ MnO_2 nanocomposites	-CDT -PDT -Hypoxia Relief -Starvation Therapy	-Mice euthanized after 14 d -Body weight & tumor volume -Histology -Serum analysis	44.134–124.072 μg/mL
Han et al., 2021 (Biomaterials)[16]	Ag_2S NPs	-PTT -Photoacoustic Imaging -Immunotherapy	-Mice euthanized after 12 d -Body weight & tumor volume -Histology -Immune profiling -Serum analysis	N/A
Wang et al., 2020 (*Biomaterials*)[17]	Cu_{2-x}Se-Au Janus NPs	-CDT -PDT -PTT -Photoacoustic Imaging -CT Imaging	-Mice euthanized after 16 d -Body weight & tumor volume -Histology	477.6–2076.8 μg/mL
Zhang et al., 2019 (*Adv. Sci.*)[18]	Honeycomb-like gold NPs	-PTT -Brachytherapy (w/ ^{125}I seeds) -Photoacoustic Imaging	-Mice euthanized after 13 d -Body weight & tumor volume -Histology	*~100 μg/mL

Li et al., 2019 (*ACS Appl. Mater. Interfaces*)[19]	Ce6 & Dox loaded hollow-CuS-1-tetradecanol NPs	-PTT -PDT -Chemotherapy -Fluorescence Imaging	-Mice euthanized after 14 d -Body weight & tumor volume -Histology	*~15–30 μg/mL
Wang et al., 2020 (*Chem. Eng. J.*)[20]	Hollow-Cu_9S_8 NPs	-CDT -PTT -Photoacoustic Imaging	-Mice euthanized after 18 d -Body weight & tumor volume -Histology -Serum analysis	N/A
Huo et al., 2017 (*Nat. Commun*)[21]	Gox-Fe_3O_4 NPs	-CDT -PTT -Starvation Therapy	-Mice euthanized after 15 d -Body weight & tumor volume -Histology	*~3–6 μg/mL
Gu et al., 2019 (*Nano. Lett.*)[22]	CuS NPs with Gefitinib	-PDT -PTT -Chemotherapy	-Mice euthanized after 22 d -Body weight & tumor volume -Histology -Serum analysis	N/A
Zhang et al., 2018 (Mater. Horiz.)[23]	Gox-Ag Nanocubes	-CDT -Starvation Therapy	-Survival analysis until tumor volume reached 2 cm^2 -Histology -Serum analysis	N/A
Zhang et al., 2021 (*Biomaterials*)[24]	PEGylated liposomes encapsulating $Fe(OH)_3$-doped CaO_2 NPs & Gox	-CDT -Starvation Therapy -Hypoxia Relief	-Mice euthanized after 16 d -Body weight & tumor volume -Histology	*~0.3 μg/mL Gox
This work	Gox-CuS NPs	-CDT -PDT -PTT -Starvation Therapy	-Mice euthanized after 14 d -Body weight & tumor volume -Histology -Serum analysis	~0.1 μg/mL CuS

N/A: Not Available/ Not Reported; CDT: chemodynamic therapy; PDT: photodynamic therapy; PTT: photothermal therapy.
*: Calculated IC values (not reported in the papers).

Supporting References

(1) Tang, Y.; Ji, Y.; Yi, C.; Cheng, D.; Wang, B.; Fu, Y.; Xu, Y.; Qian, X.; Choonara, Y. E.; Pillay, V.; Zhu, W.; Liu, Y.; Nie, Z. Self-Accelerating H_2O_2-Responsive Plasmonic Nanovesicles for Synergistic Chemo/Starving Therapy of Tumors. *Theranostics* **2020**, *10* (19), 8691–8704. https://doi.org/10.7150/thno.45392.

(2) Deng, Z.; Fang, C.; Ma, X.; Li, X.; Zeng, Y.-J.; Peng, X. One Stone Two Birds: Zr-Fc Metal–Organic Framework Nanosheet for Synergistic Photothermal and Chemodynamic Cancer Therapy. *ACS Appl. Mater. Interfaces* **2020**, *12* (18), 20321–20330. https://doi.org/10.1021/acsami.0c06648.

(3) Ma, S.; Xie, J.; Wang, L.; Zhou, Z.; Luo, X.; Yan, J.; Ran, G. Hetero-Core–Shell BiNS–Fe@Fe as a Potential Theranostic Nanoplatform for Multimodal Imaging-Guided Simultaneous Photothermal–Photodynamic and Chemodynamic Treatment. *ACS Appl. Mater. Interfaces* **2021**, *13* (9), 10728–10740. https://doi.org/10.1021/acsami.0c21579.

(4) Yang, Y.; Fan, X.; Li, L.; Yang, Y.; Nuernisha, A.; Xue, D.; He, C.; Qian, J.; Hu, Q.; Chen, H.; Liu, J.; Huang, W. Semiconducting Polymer Nanoparticles as Theranostic System for Near-Infrared-II Fluorescence Imaging and Photothermal Therapy under Safe Laser Fluence. *ACS Nano* **2020**, *14* (2), 2509–2521. https://doi.org/10.1021/acsnano.0c00043.

(5) Sun, P.; Deng, Q.; Kang, L.; Sun, Y.; Ren, J.; Qu, X. A Smart Nanoparticle-Laden and Remote-Controlled Self-Destructive Macrophage for Enhanced Chemo/Chemodynamic Synergistic Therapy. *ACS Nano* **2020**, *14* (10), 13894–13904. https://doi.org/10.1021/acsnano.0c06290.

(6) Fang, C.; Deng, Z.; Cao, G.; Chu, Q.; Wu, Y.; Li, X.; Peng, X.; Han, G. Co–Ferrocene MOF/Glucose Oxidase as Cascade Nanozyme for Effective Tumor Therapy. *Adv. Funct. Mater.* **2020**, *30* (16), 1910085. https://doi.org/https://doi.org/10.1002/adfm.201910085.

(7) Lyu, M.; Zhu, D.; Kong, X.; Yang, Y.; Ding, S.; Zhou, Y.; Quan, H.; Duo, Y.; Bao, Z. Glutathione-Depleting Nanoenzyme and Glucose Oxidase Combination for Hypoxia Modulation and Radiotherapy Enhancement. *Adv. Healthc. Mater.* **2020**, *9* (11), 1901819. https://doi.org/https://doi.org/10.1002/adhm.201901819.

(8) Zhang, D.-Y.; Huang, F.; Ma, Y.; Liang, G.; Peng, Z.; Guan, S.; Zhai, J. Tumor Microenvironment-Responsive Theranostic Nanoplatform for Guided Molecular Dynamic/Photodynamic Synergistic Therapy. *ACS Appl. Mater. Interfaces* **2021**, *13* (15), 17392–17403. https://doi.org/10.1021/acsami.1c03277.

(9) Ranji-Burachaloo, H.; Reyhani, A.; Gurr, P. A.; Dunstan, D. E.; Qiao, G. G. Combined Fenton and Starvation Therapies Using Hemoglobin and Glucose Oxidase. *Nanoscale* **2019**, *11* (12), 5705–5716. https://doi.org/10.1039/C8NR09107B.

(10) Fan, Z.; Jiang, B.; Zhu, Q.; Xiang, S.; Tu, L.; Yang, Y.; Zhao, Q.; Huang, D.; Han, J.; Su, G.; Ge, D.; Hou, Z. Tumor-Specific Endogenous FeII-Activated, MRI-Guided Self-Targeting Gadolinium-Coordinated Theranostic Nanoplatforms for Amplification of ROS and Enhanced Chemodynamic Chemotherapy. *ACS Appl. Mater. Interfaces* **2020**, *12* (13), 14884–14904. https://doi.org/10.1021/acsami.0c00970.

(11) He, S.; Jiang, Y.; Li, J.; Pu, K. Semiconducting Polycomplex Nanoparticles for Photothermal Ferrotherapy of Cancer. *Angew. Chemie Int. Ed.* **2020**, *59* (26), 10633–10638. https://doi.org/https://doi.org/10.1002/anie.202003004.

(12) Zhao, Z.; Xu, K.; Fu, C.; Liu, H.; Lei, M.; Bao, J.; Fu, A.; Yu, Y.; Zhang, W. Interfacial Engineered Gadolinium Oxide Nanoparticles for Magnetic Resonance Imaging Guided Microenvironment-Mediated Synergetic Chemodynamic/Photothermal Therapy. *Biomaterials* **2019**, *219*, 119379. https://doi.org/https://doi.org/10.1016/j.biomaterials.2019.119379.

(13) Zhang, M.; Liu, X.; Luo, Q.; Wang, Q.; Zhao, L.; Deng, G.; Ge, R.; Zhang, L.; Hu, J.; Lu, J. Tumor Environment Responsive Degradable CuS@mSiO2@MnO2/DOX for MRI Guided Synergistic Chemo-Photothermal Therapy and Chemodynamic Therapy. *Chem. Eng. J.* **2020**, *389*, 124450. https://doi.org/https://doi.org/10.1016/j.cej.2020.124450.

(14) Xiao, S.; Lu, Y.; Feng, M.; Dong, M.; Cao, Z.; Zhang, X.; Chen, Y.; Liu, J. Multifunctional FeS2 Theranostic Nanoparticles for Photothermal-Enhanced Chemodynamic/Photodynamic Cancer Therapy and Photoacoustic Imaging. *Chem. Eng. J.* **2020**, *396*, 125294. https://doi.org/https://doi.org/10.1016/j.cej.2020.125294.

(15) Zhang, L.; Yang, Z.; He, W.; Ren, J.; Wong, C.-Y. One-Pot Synthesis of a Self-Reinforcing Cascade Bioreactor for Combined Photodynamic/Chemodynamic/Starvation Therapy. *J. Colloid Interface Sci.* **2021**, *599*, 543–555. https://doi.org/https://doi.org/10.1016/j.jcis.2021.03.173.

(16) Han, R.; Xiao, Y.; Yang, Q.; Pan, M.; Hao, Y.; He, X.; Peng, J.; Qian, Z. Ag2S Nanoparticle-Mediated Multiple Ablations Reinvigorates the Immune Response for Enhanced Cancer Photo-Immunotherapy. *Biomaterials* **2021**, *264*, 120451. https://doi.org/https://doi.org/10.1016/j.biomaterials.2020.120451.

(17) Wang, Y.; Li, Z.; Hu, Y.; Liu, J.; Guo, M.; Wei, H.; Zheng, S.; Jiang, T.; Sun, X.; Ma, Z.; Sun, Y.; Besenbacher, F.; Chen, C.; Yu, M. Photothermal Conversion-Coordinated Fenton-like and Photocatalytic Reactions of Cu2-XSe-Au Janus Nanoparticles for Tri-Combination Antitumor Therapy. *Biomaterials* **2020**, *255*, 120167. https://doi.org/https://doi.org/10.1016/j.biomaterials.2020.120167.

(18) Zhang, F.; Han, X.; Hu, Y.; Wang, S.; Liu, S.; Pan, X.; Wang, H.; Ma, J.; Wang, W.; Li, S.; Wu, Q.; Shen, H.; Yu, X.; Yuan, Q.; Liu, H. Interventional Photothermal Therapy Enhanced Brachytherapy: A New Strategy to Fight Deep Pancreatic Cancer. *Adv. Sci.* **2019**, *6* (5), 1801507. https://doi.org/https://doi.org/10.1002/advs.201801507.

(19) Li, Q.; Sun, L.; Hou, M.; Chen, Q.; Yang, R.; Zhang, L.; Xu, Z.; Kang, Y.; Xue, P. Phase-Change Material Packaged within Hollow Copper Sulfide Nanoparticles Carrying Doxorubicin and Chlorin E6 for Fluorescence-Guided Trimodal Therapy of Cancer. *ACS Appl. Mater. Interfaces* **2019**, *11* (1), 417–429. https://doi.org/10.1021/acsami.8b19667.

(20) Wang, Y.; An, L.; Lin, J.; Tian, Q.; Yang, S. A Hollow Cu9S8 Theranostic Nanoplatform Based on a Combination of Increased Active Sites and Photothermal Performance in Enhanced Chemodynamic Therapy. *Chem. Eng. J.* **2020**, *385*, 123925. https://doi.org/https://doi.org/10.1016/j.cej.2019.123925.

(21) Huo, M.; Wang, L.; Chen, Y.; Shi, J. Tumor-Selective Catalytic Nanomedicine by Nanocatalyst Delivery. *Nat. Commun.* **2017**, *8* (1), 357. https://doi.org/10.1038/s41467-017-00424-8.

(22) Gu, X.; Qiu, Y.; Lin, M.; Cui, K.; Chen, G.; Chen, Y.; Fan, C.; Zhang, Y.; Xu, L.; Chen, H.; Wan, J.-B.; Lu, W.; Xiao, Z. CuS Nanoparticles as a Photodynamic Nanoswitch for Abrogating Bypass Signaling To Overcome Gefitinib Resistance. *Nano Lett.* **2019**, *19* (5), 3344–3352. https://doi.org/10.1021/acs.nanolett.9b01065.

(23) Zhang, Y.; Yang, Y.; Jiang, S.; Li, F.; Lin, J.; Wang, T.; Huang, P. Degradable Silver-Based Nanoplatform for Synergistic Cancer Starving-like/Metal Ion Therapy. *Mater. Horizons* **2019**, *6* (1), 169–175. https://doi.org/10.1039/C8MH00908B.

(24) Zhang, X.; He, C.; Chen, Y.; Chen, C.; Yan, R.; Fan, T.; Gai, Y.; Yang, T.; Lu, Y.; Xiang, G. Cyclic Reactions-Mediated Self-Supply of H2O2 and O2 for Cooperative Chemodynamic/Starvation Cancer Therapy. *Biomaterials* **2021**, *275*, 120987. https://doi.org/https://doi.org/10.1016/j.biomaterials.2021.120987.